

Optimization of Green Synthesis of Zinc Oxide Nanoparticles Using *Rosa damascena* Residue via Box-Behnken Design and Assessment of their Environmental Activity

Imane Adraoui^{1,2,*} , Nabil Saffaj¹ , Rachid Mamouni¹ , Si Mohamed Jadoualia^{1,3}

¹ Team of Biotechnology, Materials and Environment, Faculty of Sciences Agadir, Ibn Zohr University, Morocco;

² Faculty of Applied Sciences-Ait Melloul, Ibn Zohr University, Morocco;

³ Laboratory of Biotechnology, Bioresources and Bioinformatics, EST Khenifra, Sultan Moulay Sliman University, Morocco;

* Correspondence: i.adraoui@uiz.ac.ma

Received: 23.09.2024; Accepted: 15.07.2025; Published: 30.09.2025

Abstract: The fight against water pollution has received particular attention and is one of the most pressing environmental concerns, given that water is susceptible to pollution. Therefore, it is necessary to create new, eco-friendly technology for wastewater treatment. The present study used the dry rose waste (*Rosa damascena*) extract as a capping and reducing agent to initiate the nucleation and structure of ZnO NPs. To our knowledge, the synthesis of ZnO NPs using a rose waste (*Rosa damascena*) extract and their properties as a novel green approach are not well documented. Furthermore, this study is considered a simple, cost-effective, and environmentally friendly alternative to chemical and physical procedures. However, the Response Surface Methodology (RSM) based on the Box–Behnken Design (BBD) has been used to optimize conditions for the synthesis of ZnO nanoparticles. The optimal factors for synthesizing ZnO NPs using BBD were found to be the mass of the plant, 20 g, the salt concentration of 0,2, and the calcination temperature of 500°C. Next, various techniques, including X-ray diffraction, scanning electron microscopy, and UV-visible spectroscopy, were used to confirm the formation of ZnO NPs. The results showed that ZnO NPs had a better effect on photodegradation activity in treating aqueous solutions containing orange G dyes after 120 minutes under sunlight irradiation.

Keywords: zinc oxide nanoparticles; green synthesis; *Rosa damascena*; plant extracts; dye degradation; Box–Behnken design.

© 2025 by the authors. This article is an open-access article distributed under the terms and conditions of the Creative Commons Attribution (CC BY) license (<https://creativecommons.org/licenses/by/4.0/>), which permits unrestricted use, distribution, and reproduction in any medium, provided the original work is properly cited. The authors retain copyright of their work, and no permission is required from the authors or the publisher to reuse or distribute this article, as long as proper attribution is given to the original source.

1. Introduction

The scientific community has focused on utilizing nanotechnology for environmental protection and long-term sustainability, as it is one of the most significant new trends in the environmental protection sector, notably in waste management. Additionally, nanotechnology has been used in several fields and industries, including health and food safety, as well as in many aspects of daily life [1,2]. Several studies have demonstrated that using green chemistry to manufacture metal nanoparticles using plant extracts is a relatively recent development in sustainability. Additionally, this topic has drawn a lot of interest since it can create alternative, safer, more energy-efficient, environmentally eco-friendly, and less hazardous methods [3–6].

However, using waste as raw materials to promote the circular economy can also help the environment. This device employs extracts from various plant sections during synthesis as reducing and capping agents [7].

Rosa damascena, frequently referred to as "damask rose," is one of the more valuable rose species in Morocco [8]. The damask rose is cultivated in the M'goun-Dades valleys for its watering and oil extraction and contains various components, e.g., flavonoids including (catechin and epicatechin), phenolic acids including (chlorogenic and ferulic) and glycosides that have valuable effects. Therefore, roses have various uses depending on the species and varieties, so for the production of a small volume of rose water, a large quantity of rose flower products is needed [8–13]. In light of this, significant amounts of solid trash are produced, which could lead to environmental pollution in nearby locations. The analysis and characterization of the rose waste biomass showed that a large portion of the polyphenols and phenolic compounds remained unextracted and indicating that additional research was required for the reuse of waste, waste reduction, and obtaining a valuable product [14,15]. Furthermore, waste (rose waste) can be recycled and converted into useful and efficient nano-biosorbents and their application in textile wastewater treatment [16].

The use of green chemistry for the synthesis of metal nanoparticles using plant extracts is a relatively new and emerging issue regarding sustainability. However, extracts of various plant parts have been used as effective chelating agents. For this reason, ZnO NPs have been synthesized using green chemistry processes and have been utilized in numerous innovative optical and electronic products because of their characteristics [17–19]. Zinc oxide nanoparticles have a wider surface area, smaller band gap, and smaller particles, which accelerate UV-light absorption and photodegradation [20,21]. The ZnO nanoparticles have been investigated widely for their effective role in biological systems, medicine, pharmaceutical, and food industries, as well as their photodegradation activity for different types of organic dyes or other wastes from contaminated surface water. As a result, ZnO NPs have drawn a lot of interest in the process of degrading and mineralizing environmental contaminants [17,22–24], given the potential of ZnO nanoparticle systems and the environmental advantages of green synthesis. Many experiments are required to analyze the effect of many parameters and their common interaction on the quantity and properties of ZnO [25–27]. Experimental design is commonly used to reduce the number of trials and to determine a response value for any usual variables chosen from the experimental areas under study. Response surface methodology (RSM) has been successfully applied to various extraction processes, industrial sectors, and research fields to optimize operating parameters for specific processes. It is a statistically reliable methodology for studying the interactions between dependent and independent variables and predicting the resulting responses in the presence of specific circumstances [28–30]. The basic principle of RSM is to use a series of pre-planned experiments to discover the best possible answer. There are two types of RSM methods, namely central composite design (CCD) and Box–Behnken design (BBD). In this study, we used the BBD because of the relatively few experimental runs required, making BBD more efficient and effective than CCD. The response surface approach, founded on the Box-Behnken design (BBD) was used to explore the effect of operating factors on the synthesis of zinc oxide nanoparticles. According to our research, these designs have never been used to optimize ZnO nanoparticle production. Thus, within the scope of this study, we synthesized ZnO nanoparticles based on *Rosa damascena* waste extracts as a reducing and stabilizing agent without the addition of any acid or base standard component based on a simple, cost-effective,

and sustainable green approach, and we applied the above designs BBD to determine the optimum conditions to obtain the maximum mass of zinc oxide nanoparticles. Furthermore, one of the environmental concerns and challenges is textile dye wastewater. Several studies have shown that effluents containing this dye must be treated before being discharged into the environment [31]. To overcome this problem, this study focused on exploring the photocatalytic activity prowess of ZnO NPs based on *Rosa damascena* waste extracts, specifically in the degradation of orange G dye after 120 minutes under sunlight. Lastly, this research highlights the commitment to address pressing environmental challenges through nanoparticle technology and innovative sustainable synthesis methods.

2. Materials and Methods

2.1. Chemicals and reagents.

The entire chemical employed in this work was of analytical grade, acquired from Sigma-Aldrich, and used without further purification. Zinc nitrate hexahydrate ($\text{Zn}(\text{NO}_3)_2 \times 6\text{H}_2\text{O}$) from Sigma-Aldrich (99.99% purity), and all the solutions were produced using deionized water as the synthesis medium.

2.2. Preparation of *Rosa damascena* extract.

In our experiment, the dry rose watering wastes (*Rosa damascena*) were collected from the “*M'goun-Dades*” valleys and washed properly to remove any dust or unwanted particles. The extract was prepared using the dry rose waste, chosen for its high content of desired organic compounds, by mixing different quantities (5 g, 10 g, and 20 g) of the waste in 100 ml of deionized water for 24 hours at room temperature. The solution was then filtered using filter paper (Whatman No.1), and the filtrate was stored at 4°C for further use.

2.3. Green synthesis of ZnO nanoparticles using *Rosa damascena* extract.

Different solutions of the resulting filtrate (5 g, 10 g, and 20 g) were used as reducing agents for ZnO NP synthesis. In 100 ml of rose extract, 6 g of zinc precursor salt ($\text{Zn}(\text{NO}_3)_2 \times 6\text{H}_2\text{O}$) was dissolved under agitation to dissolve the Zn salt completely. The brown residue was gathered by centrifugation, washed several times with bi-distilled water, and dried for 24 hours in a 70°C oven. The resultant powder was calcined at 500°C for 30 minutes before being stored for characterization. The process by which plant extracts produce nanoparticles, as well as the biomolecules in charge of that process, is still not fully understood [25]. Biomolecules that generate ZnO nanoparticles, such as flavonoid leaf extracts, may lose electrons to effectively convert Zn^{2+} ions to Zn^0 . This may result in the Zn^0 phenolate complex by having a chelating effect that causes NPs to form and develop at 70°C. This compound decomposes at a higher temperature of 100°C in reducing Zn NPs [30]. Therefore, the phenolic compounds had valuable effects on the formation of ZnO NPs.

2.4. Experimental design.

The RSM with Box-Behnken Design (BBD) was used to acquire details about the significant impacts and to investigate probable interactions between the selected significant factors that have a beneficial effect on the synthesis of ZnO NPs, as well as to find the ideal value of each factor. A three-factorial Box-Behnken experimental design with three levels was

used in this study. The levels of the factors were -1 (low), 0 (center point), and 1 (high). During the optimization phase, an empirical model was established to associate the response of the ZnO NPs synthesis process, which is based on the second-order quadratic model given in the following equations, Eq. (1) and Eq. (2):

$$Y = b_0 + \sum_{i=1}^k b_i X_i + \sum_{i=1}^K b_{ii} X_i^2 + \sum_{i=1}^k \sum_{j=1}^K b_{ij} X_i X_j + \varepsilon \quad (1)$$

$$Y = b_0 + b_1 X_1 + b_2 X_2 + b_{12} X_1 X_2 + b_{11} X_1^2 + b_{22} X_2^2 \quad (2)$$

Where (Y) is the response, b_0 is a constant, b_i is the linear coefficient, (b_{ij}) is the interaction coefficient, (b_{ii}) is the quadratic coefficient, (X_i) is the level of the coded variable, and (i) or (j) is the number of variables with independent values. The BBD was investigated through 15 experiments for the production of ZnO NPs, and a matrix was studied at the highest level (1) and the lowest level (-1). Table 1 displays the coded values of the variables together with the response of ZnO NPs. The P-value at a 95% confidence level was utilized to determine the predominant influence of ZnO NPs.

Table 1. Independent Variables and Their factor levels for the optimal Box–Behnken Design.

Independent Variables	Range and level		
	Low (-1)	Central (0)	High (+1)
Salt concentration (SC) (mol/l)	0,05	0,125	0,2
Calcination temperature (ST) (°C)	300	400	500
Mass plant (MP) (g)	5	12,5	20

2.5. Characterization techniques of ZnO nanoparticles.

The optical absorption of green ZnO nanoparticles was measured using UV-Vis spectroscopy at room temperature. The diffraction pattern of the sample was identified using X-ray diffraction (XRD) on a powder Empyrean Panalytical diffractometer at an irradiation wavelength of 1.5480 Å (Cu K α) in the angular range of 15-90 with a scan step size of 0.034. The structural morphology of the resultant ZnO NPs was examined by SEM combined with EDS analysis by JEOL (JSM-IT200).

2.6. Photocatalytic activity of ZnO nanoparticles.

The photodegradation of the pollutant dye Orange G by green synthesized ZnO NPs was tested under sunlight. 0.4 g/l of prepared ZnO NPs were supplementary added to an aqueous solution of Orange G (10^{-2} g/l) and was sonicated to ensure homogeneous dispersion. The resulting suspension was placed in the dark and stirred for 30 minutes. After equilibrium t_0 , the suspension was exposed to solar irradiation under stirring from 11h00 to 14h00. To obtain the absorption spectra, 4 ml of suspension was regularly withdrawn every 10 minutes using a disposable syringe, centrifuged to separate phases (OG and NPs), and analyzed using UV-Vis between 300 nm and 800 nm.

3. Results and Discussion.

3.1. Optimum conditions for green synthesis of ZnO nanoparticles.

Three variables of salt concentration, plant mass, and calcination temperature were selected for the optimization process to form synthesized ZnO nanoparticle powder, which are displayed in Table 2. Through the experimental process, the Box Behnken design generated a

regression equation for each element at a 5% significance level. However, the analysis of variance ANOVA and plots of observed values against anticipated results were used to confirm the model's validity, and the interaction effect of the chosen parameters on the response observed [29,32]. From this analysis, we also obtained the following mathematical model of mass synthesis ZnO NP (Y1):

$$Y_1 = 302,67 + 69,38A + 52,50 B - 0,62 C - 8,83 A. A - 2,58 B. B - 1,33 C. C + 23,75 A. B + 5,00 A. C + 1,25 B. C \quad (3)$$

Table 2. The experiment design matrix and Box-Behnken measured values of the considered responses.

Run	Coded values			Experimental values			Experimental response	predicted responses
	A	B	C	SC mol/l (A)	ST (°C) (B)	MP (%) (C)	Y1 (mg) m(ZnO)	Y1(mg) m(ZnO)
1	0	1	1	0,125	500	20	350	351,875
2	1	-1	0	0,2	300	12,5	275	284,375
3	0	0	0	0,125	400	12,5	300	302,666667
4	0	-1	1	0,125	300	20	245	244,375
5	-1	-1	0	0,05	300	12,5	200	193,125
6	1	1	0	0,2	500	12,5	430	436,875
7	1	0	1	0,2	400	20	375	366,25
8	1	0	-1	0,2	400	5	365	357,5
9	-1	0	-1	0,05	400	5	220	228,75
10	-1	1	0	0,05	500	12,5	260	250,625
11	0	0	0	0,125	400	12,5	305	302,666667
12	0	1	-1	0,125	500	5	350	350,625
13	0	-1	-1	0,125	300	5	250	248,125
14	0	0	0	0,125	400	12,5	303	302,666667
15	-1	0	1	0,05	400	20	210	217,5

(Y1: Mass of ZnO NPs (mg)) SC: Salt concentration; ST: Calcination temperature; MP: Mass plant.

Regression models for (Y1) were developed based on the experimental data, following Eq. (3). The suitability of the first model was assessed using a parity diagram between observed and predicted values, illustrated in Figure 1. As shown in Figure 2, the high values of the correlation coefficient ($R_2=0.99$) for masse (ZnO) indicate an excellent correlation between observed and predicted responses by the first models.

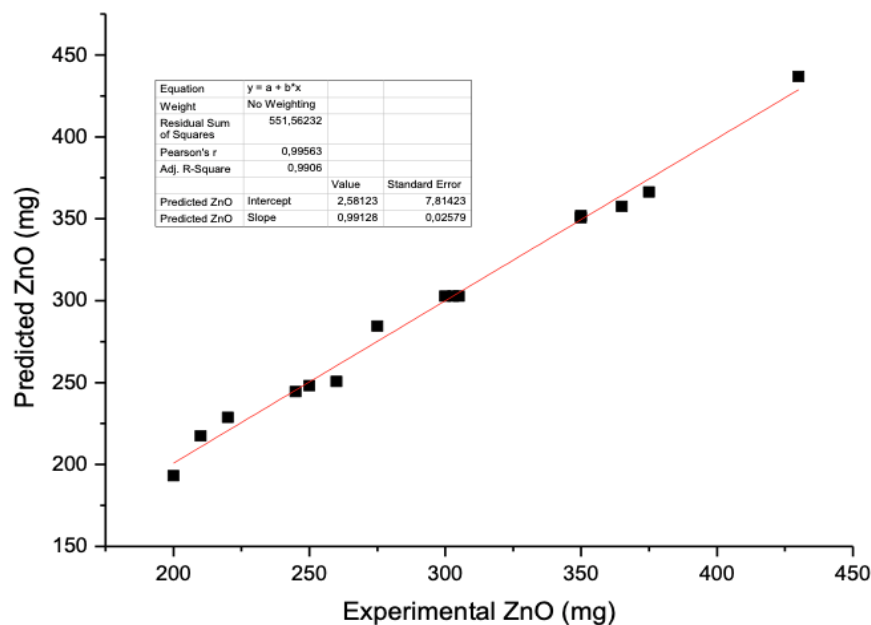


Figure 1. Plot of the model-predicted versus observed response of ZnO synthesis responses.

The applicability and significance of the model were explored using analysis of variance (ANOVA). The effect of a factor is described as the change in reaction caused by a shift in the factor's concentration. This is commonly referred to as the major effect because it pertains to the tests' most interesting parts. The ANOVA results demonstrated that the equation effectively described the real connection between each response and the important variables. The F-value indicates that the models are significant, and a Prob>F value less than 0.05 suggests that the model's terms are significant. A higher F-value with a lower P-value (less than 0,05, confidence intervals) indicates that the experimental system can be represented well with less error. Based on the ANOVA results presented in Table 3, the values of F-cal (63,12 for ZnO NPs (Y1) were greater, and P values were less than 0,05, indicating the significance and applicability of the BBD model terms. Furthermore, Figure 2 depicts the relationship between the normal probability and the residuals. The normal probability of the residuals nearly revealed no deviations from normality. Because of the low p-value ($P < 0.05$) for the factors, the linear effect and two interactions of salt concentration and calcination temperature were expected to have the most impact of all the terms. Meanwhile, the quadratic was not of statistical significance in the synthesis of ZnO NPs. The multiple correlation coefficient (R^2) and adjusted R^2 were used to evaluate the fitness of the equation. As indicated in Table 4, the high coefficient of determination (R^2 : 0,991) and modified coefficient of determination (R^2 adj: 0,975) demonstrate the relationships and interactions between experimental variables and projected response values. The projected R-squared (R^2 pred: 0,863) agreed with the adjusted R-squared and demonstrated a satisfactory prediction of the model.

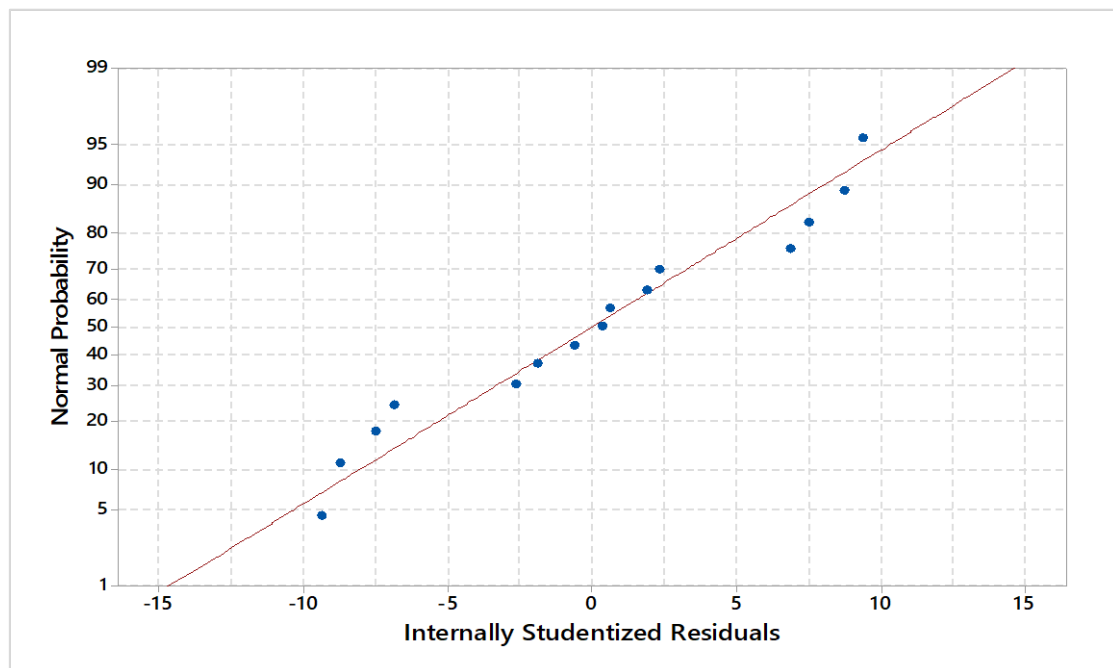


Figure 2. Normal probability of the residuals of ZnO NPs.

Table 3. ANOVA for the response surface in the prediction of ZnO synthesis.

Source	The sum of square (SS)	df	Mean squares (MSS)	F Value	P-value probability (P)>F
Model	63221,3	9	7024,6	63,12	0,000
Linearity	60556,2	3	20185,4	181,39	0,000
Salt Concentration (mol/l)-A	38503,1	1	38503,1	345,99	0,000
Calcination Temperature (°C)-B	22050,0	1	22050,0	198,14	0,000

Source	The sum of square (SS)	df	Mean squares (MSS)	F Value	P-value probability (P)>F
Mass Plant (mg)-C	3,1	1	3,1	0,03	0,873
Square	302,6	3	100,9	0,91	0,500
A*A	288,1	1	288,1	2,59	0,169
B*B	24,6	1	24,6	0,22	0,658
C*C	6,6	1	6,6	0,06	0,818
2-way interaction	2362,5	3	787,5	7,08	0,030
A*B	2256,2	1	2256,2	20,27	0,006
A*C	100,0	1	100,0	0,90	0,387
B*C	6,2	1	6,2	0,06	0,822
Error	556,4	5	111,3	-	-
Lack-of-Fit	543,7	3	181,2	28,62	0,034
Pure Error	12,7	2	6,3	-	-
Total	63777,7	14	-	-	-

Table 4. Correlation coefficient (R2) values corresponding to the used models.

Response	R ² coefficient of determination	R ² adjusted	R ² predicted
Y1: ZnO NPs (mg)	0,991	0,975	0,863

Factorial diagrams were used to evaluate the factors influencing pore diameter (nm) [28,29,33,34]. Taking into account the value of the linear coefficient supplied in the preceding equations, the weight effect of the analyzed parameters followed the order: A>B>C for ZnO NP synthesis. As illustrated in Figure 3, the major effect used to evaluate which factors most influence each parameter's response indicates deviations from the average between high and low values of each one.

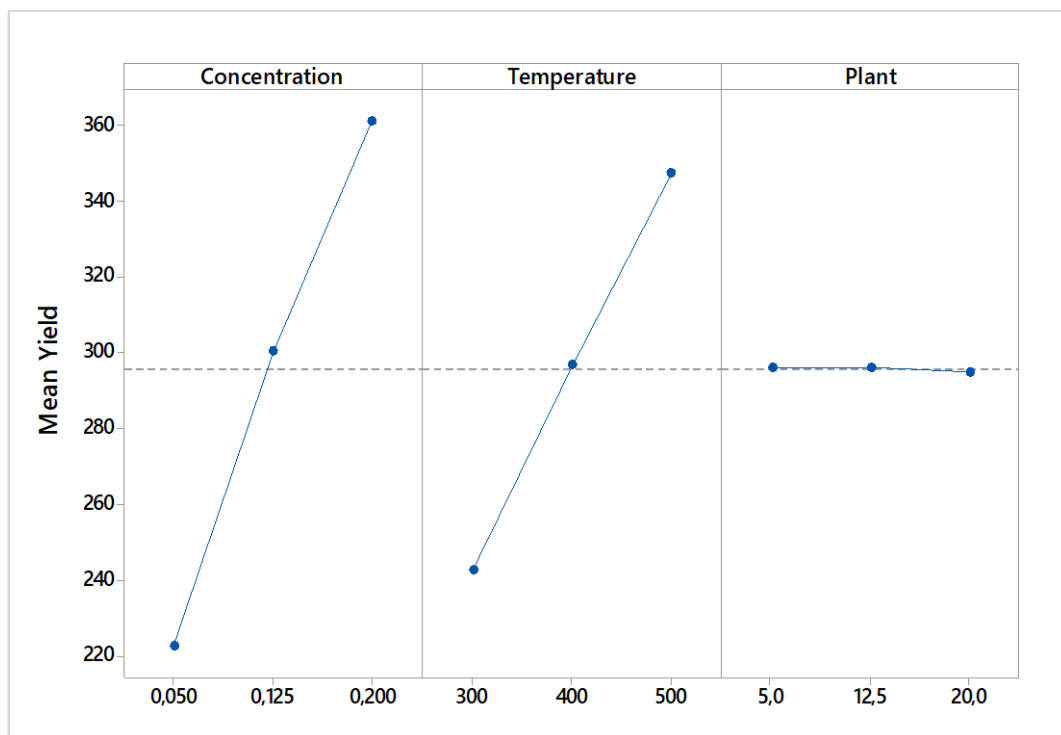


Figure 3. Results of main effects for pore diameter of ZnO nanoparticles.

3.2. Response optimization.

The synthesis ZnO nanoparticle diameter and the response surface plot variables are shown in three-dimensional surface plots in Figure 4 versus temperature and concentration. However, each level of a component has a different effect on the response; when the slope is close to zero, the magnitude of the primary effects will be minor. The obtained data demonstrate that the salt concentration had a significant impact on the response of the pore

diameter, as demonstrated by the steep slope due to the large surface area, followed by the calcination temperature and plant mass. In the case of salt concentration, a steep slope suggests that even minor changes in salt concentration have a substantial effect on the reaction, most likely due to its function in surface characteristics. ZnO production and structure may be affected by salt concentration, leading to a change in pore diameter. If the slope of a factor, such as calcination temperature, is near zero, it implies that temperature variations have little impact on the reaction. This could indicate that variations in calcination temperature do not significantly affect pore diameter within the examined temperature range. As depicted in Figure 4, the graphical interaction between salt content and calcination temperature that raising the calcination temperature and salt concentration enhanced the mass of synthesis ZnO.

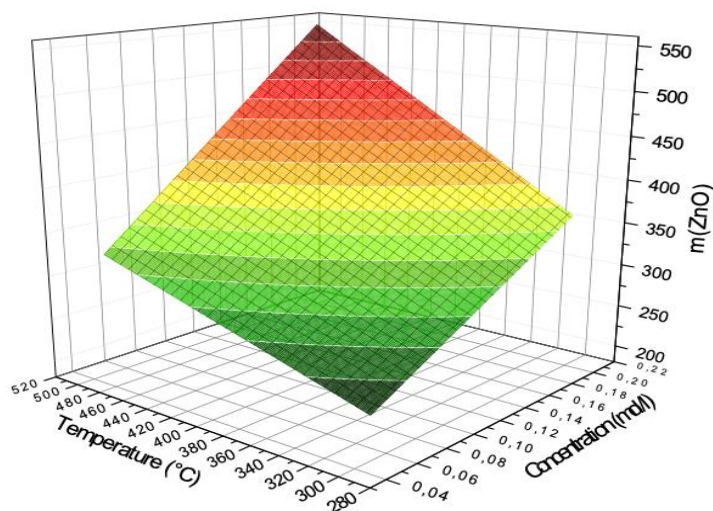


Figure 4. Response surface plot of ZnO NPs synthesis vs. temperature and concentration.

The goal of the response optimization for the current model was to maximize the mass synthesis of ZnO nanoparticles. The optimal predicted response to the production of 430 mg ZnO nanoparticles contains a salt concentration of 0.2 mol/l, a calcination temperature of 500°C, and a plant mass of 20 mg.

3.3. Characterization of ZnO nanoparticles at optimized conditions.

3.3.1. X-ray diffraction.

The XRD analysis of the ZnO NPs produced by using an extract of different amounts (5 g, 10 g, and 20 g) of waste rose as a reducing agent, then annealed at 500°C for 30 minutes, is displayed in Figure 5. At room temperature, the sample was obtained in the angular range of $2\theta=05-60^\circ\text{C}$. The tree sample XRD pattern shown in Figure 3 has 13 diffraction peaks that are assigned to scattering from the crystallographic planes (100), (002), (101), (102), (110), (103), (200), (112), (201), (004), (202), (104), and (203), with no impurity peaks. The diffraction peaks were attributed to the wurtzite (hexagonal) structure of ZnO using the standard (JCPDS Card No. 96-900-8878), and the peaks are broad and weak, confirming that the synthesized ZnO NP is very pure and nanocrystalline.

Using diffraction peaks and Scherrer's formula, the average crystallite size of ZnO NP was determined to be 32 nm [32,35]. The average values of the hexagonal ZnO lattice parameters a and c were determined using the plane distances relation [34].

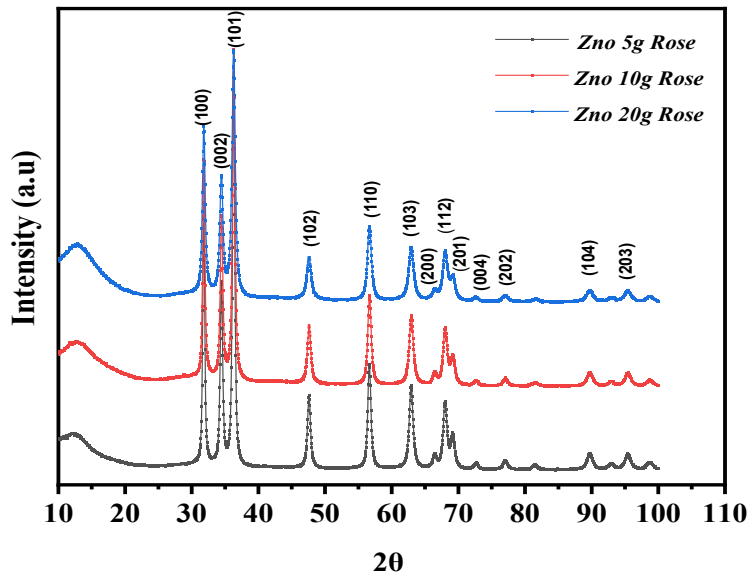


Figure 5. The intensity vs. 2θ profile obtained for the ZnO NPs prepared from aqueous extracts of wastes (*Rosa damascena*) at a) 5g, b) 10 g, and c) 20g.

$$d_{hkl} = \left[\frac{4(h^2 + hk + k^2)}{3a^2} + \frac{l^2}{c^2} \right]^{-1/2} \quad (4)$$

The mean value of the lattice parameters as determined by equation (4) is ($a = 0.3249$ nm and $c = 0.5207$ nm), and these values are in agreement with those of the wurtzite structure of ZnO. The c/a ratio is almost not dependent on the type of natural extract of Damask Rose, and the crystallite size was determined using the Debye-Scherrer equation (5), which is given as [36]:

$$D = \frac{0.9\lambda}{\beta \cos\theta} \quad (5)$$

Where D is crystallite size, λ is the incident wavelength of the X-ray, while β (in radians) is line broadening at half the maximum intensity, and θ is Bragg’s angle. The average D is found to be 20.2 nm, 20.3 nm, and 20.4 nm, respectively, for ZnO-NPs synthesized by 5 g of Rose, 10 g of Rose, and 20 g of Rose. Therefore, the ZnO-NPs structural properties prepared in the three samples of rose extract give similar results compared to the others, and this combination is likely influenced by the molecular compounds of rose waste.

Furthermore, literature reports indicate that zinc nanoparticles synthesized by plant extract are stable over the long term. Additionally, due to their potential to reduce, phytochemicals from plants also interact with the surface of the particle and help stabilize the nanoparticles [6,37].

Table 5. Average lattice parameters.

	a (Å)	c (Å)	c/a
ZnO 5g Rose	3.249	5.207	1.602
ZnO 10g Rose	3.249	5.207	1.602
ZnO 20g Rose	3.249	5.207	1.602

3.3.2. Scanning electron microscopy (SEM).

The SEM microstructure of green synthesized ZnO nanoparticles (5 g, 10 g, and 20g) are displayed in Figure 6(a), (b), and (c), respectively. The SEM depicts that the particle shapes

were spherical, with diameters varying between 0.11 μm and 0.33 μm , which were consistent with the crystallite size calculated by Scherrer's formula using diffraction peaks observed in XRD spectra. Nanoparticles with particle sizes of 0.21-0.30 μm exhibit more strain (confirmed by lattice strain calculation) than nanoparticles with particle sizes of less than 0.50 μm [38,39]. The results obtained for 20 g of rose waste show large clusters of zinc oxide particles. The agglomeration of the particles during the precipitation of the solution may be the cause of the creation of such massive clusters. As a result of the lack of toxic chemicals, such as expensive capping agents, this method is both environmentally friendly and cost-effective. The phytochemicals found in rose waste extract act as capping and reducing agents, and are responsible for the reduced agglomeration. Metal salts are transformed into metal oxide nanoparticles by the phytochemicals of flavonoids and phenolic compounds [35,40,41]. However, the elementary EDS mapping images presented in Figure 7 indicate the atomic percentages of elements Oxygen (16.30%) and Zinc (83.7%) and explain the presence of ZnO NPs.

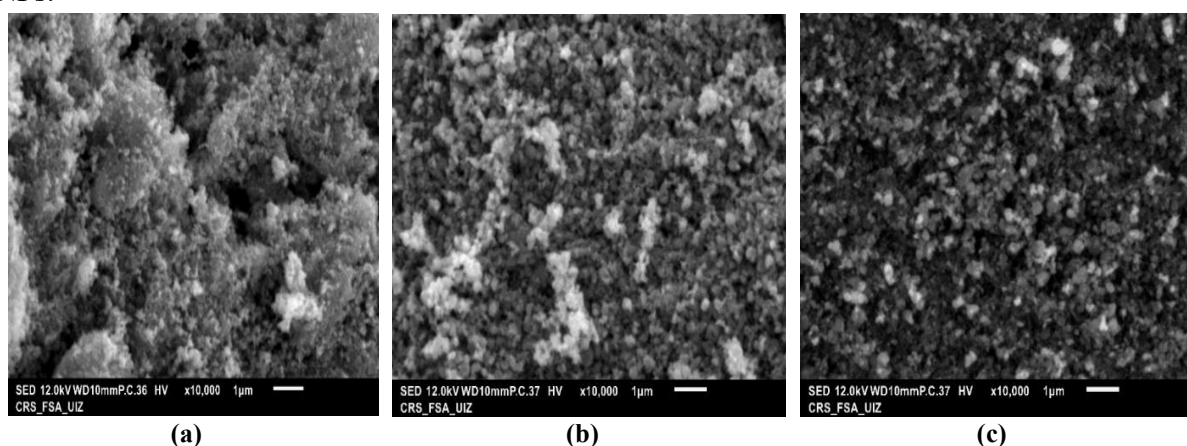


Figure 6. SEM images of the ZnO nanoparticles synthesized with (a) 5 g; (b) 10 g; (c) 20g of Rose waste.

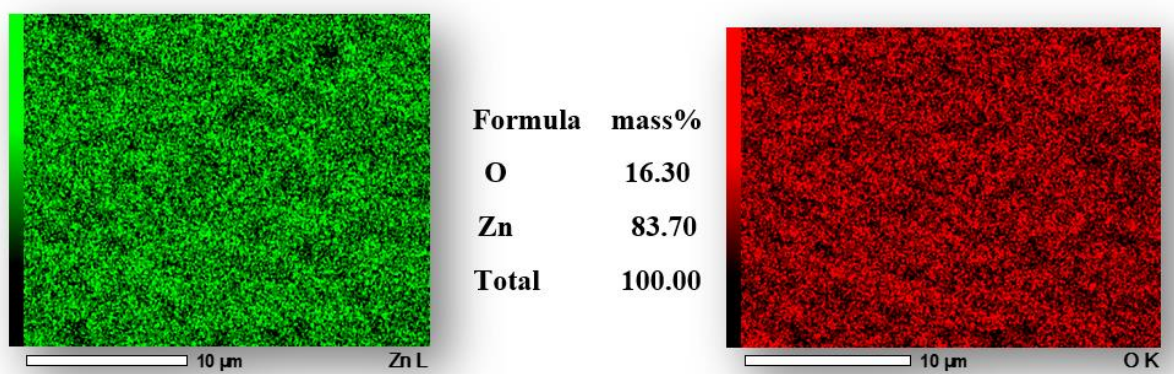


Figure 7. EDS mapping shows the distribution of oxygen and zinc elements in the ZnO NPs.

3.3.3. UV-visible spectroscopy.

UV-visible spectroscopy was used to investigate the optical properties of ZnO nanoparticles in the range of 300–600 nm wavelengths. The prepared sample of ZnO nanoparticles was ultrasonicated separately with deionized water for 5 min to obtain homogeneous solutions. Figure 8 displays the UV-Vis absorption spectra of ZnO nanoparticles produced at optimized conditions, and the ZnO nanoparticles show a clear absorption band at about 375 nm. The specific absorption peak is related to the restricted particle size distribution and monodispersity of the generated ZnO particles, and the energy gap widens due to their quantum size effects.

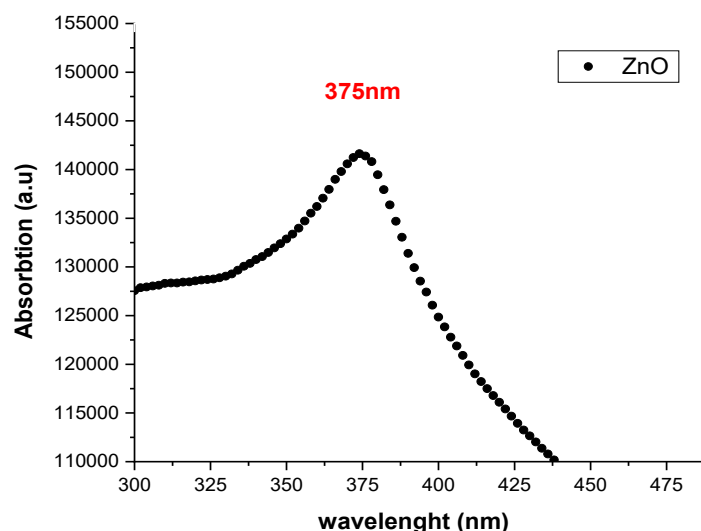


Figure 8. UV–visible spectra of ZnO nanoparticles prepared by Rosa damascena extract.

In addition, there are no additional peaks in the UV-visible spectrum, indicating their high purity. Green synthesized ZnO nanoparticles have a band gap energy value of 3.31 eV, which is induced by intragap and quantum confinement states [35]. ZnO is another effective photocatalyst with strong UV absorption properties. It can degrade organic pollutants in wastewater by generating hydroxyl radicals and superoxide anions upon light irradiation.

3.4. Photocatalytic activity of ZnO NPs.

Photocatalytic activity on wastewater, enhanced by nanotechnology, represents a promising approach to addressing wastewater treatment challenges. Advanced nanomaterials serve as photocatalysts by improving pollutant degradation efficiency and effectiveness, furthering sustainable development goals, and preserving the environment [42]. Furthermore, Figure 9 shows that oxygen molecules adsorbed on the surface also react with photogenerated electrons to form radicals that act as powerful oxidants for the decomposition of organic dyes, namely superoxide O_2^- , hydroperoxyl OH_2 and hydroxyl OH^- under sunlight irradiation. Because of their response to visible light, ZnO can be excited to produce e^- and h^+ simultaneously.

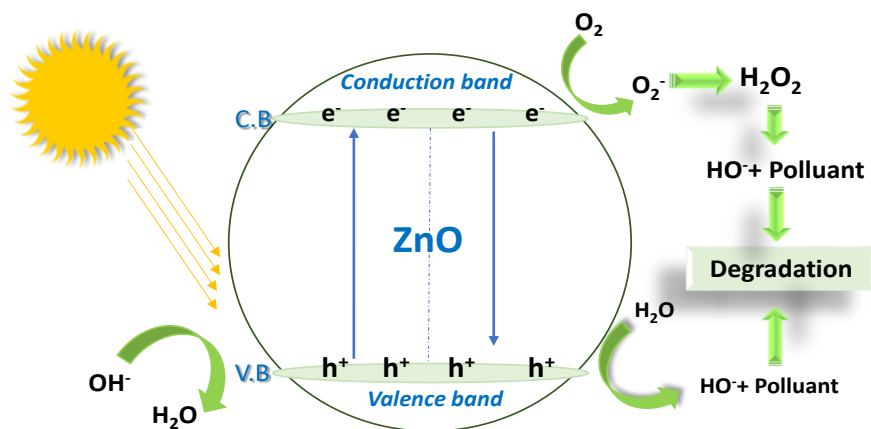


Figure 9. Photocatalytic mechanism of ZnO nanoparticles.

The degradation of orange G as a model pollutant under sun irradiation for 120 min served as an evaluation of the ZnO NPs' photocatalytic activity, as shown in Figure 10 (a). Temporal variations in Orange G dye concentration are monitored by detecting the variation

of maximum absorbance in the UV-vis spectra at 475 nm. The optical absorbance (A) of OG dye was significantly increased by 0.1 (a.u.) for 120 min under solar irradiation. This may be due to the incomplete dissolution of the OG dye in the aqueous solution, which means that the filtration step is significant before testing [22,43,44]. However, the photodegradation of OG dye using the synthesized ZnO was investigated, as shown in Figure 9; the intensity of the OG dye decreases gradually with increasing time, indicating a significant orange G degradation rate calculated using the formula (6), and the degradation of Orange G pollutants under UV light with a catalytic activity of ~56 % at 120 min Figure 10 (b).

$$D (\%) = A_0 - A / A_0 \times 100 \quad (6)$$

Where D denotes the degradation rate and A_0 and A_t denote the absorbance at time t (0 min) and time t (t), respectively.

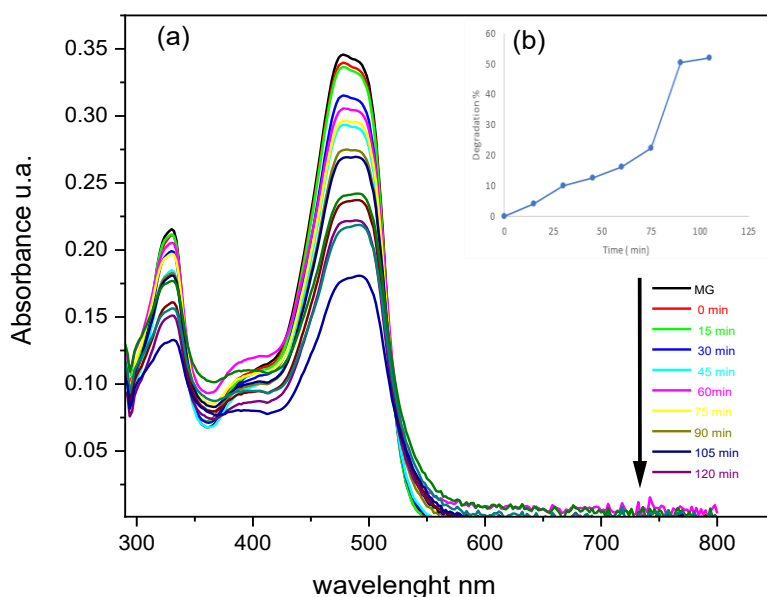


Figure 10. (a) Absorption spectra of photodegradation of Orange G using green ZnO NPs at Solar irradiation time; (b) Photocatalytic degradation (D%) of Orange G vs time.

4. Conclusions

In this study, Rosa damascena extracts were used as reducing and stabilizing agents in a simple and low-cost method for producing zinc oxide nanoparticles. The experimental setup was optimized and estimated using Design Expert software. Three variable factors, such as salt concentration, calcination temperature, and mass Plant were modeled using the response surface methodology (RSM) based on the Box–Behnken design (BBD) and were used to optimize the synthesis of ZnO-NPs.

The synthesized ZnO-NPs nanoparticles were examined using UV-vis, XRD, and SEM analysis methods. The average particle size, as determined by the Scherer formula, was found to be between 25 and 50 nm. Particles in the 85-100 nm range have an erratic morphology, according to SEM pictures. Our findings also point to a significant relationship between Orange G photodegradation and the oxygen atoms of ZnO. However, the use of ZnO nanoparticles will reduce energy and waste management costs while improving process effectiveness. However, photodegradation is set to be a key element of a cleaner, more sustainable future as long as research and development in this field continue. As an alternative to physicochemical approaches, producing ZnO-NPs using rose Damascus can be a more affordable and

ecologically friendly solution. Furthermore, for optimization of the process, the results of the pollution management available test can be used to synthesize ZnO-NPs for large-scale production in several applications.³

Author Contributions

Conceptualisation, I.A.; Methodology, I.A., N.S.; Software: N.S.; Validation, I.A., N.S.; Formal analysis, I.A., N.S., R.M., S.M.J.; Investigation, I.A., N.S.; Resources, R.M., S.M.J.; Data curation, I.A., N.S.; Writing – original draft preparation, I.A., N.S.; Writing—review and editing, I.A., N.S.; Visualization, I.A., N.S.; Supervision: I.A., N.S. All authors have read and agreed to the published version of the manuscript.

Institutional Review Board Statement

Not applicable

Informed Consent Statement

Not applicable

Data Availability Statement

Data supporting the findings of this study are available upon reasonable request from the corresponding author.

Funding

This research received no external funding.

Acknowledgments

The authors gratefully acknowledge the TBME team for their kind support and for providing access to instrumental facilities at the Faculty of Sciences, IBN Zohr University, Agadir.

Conflicts of Interest

The authors declare no conflict of interest.

References

1. Brar, K.K.; Magdoui, S.; Othmani, A.; Ghanei, J.; Narisetty, V.; Sindhu, R.; Binod, P.; Pugazhendhi, A.; Awasthi, M.K.; Pandey, A. Green route for recycling of low-cost waste resources for the biosynthesis of nanoparticles (NPs) and nanomaterials (NMs)-A review. *Environ. Res.* **2022**, *207*, 112202, <https://doi.org/10.1016/j.envres.2021.112202>.
2. Dermatas, D.; Mpouras, T.; Panagiotakis, I. Application of Nanotechnology for waste management: Challenges and limitations. *Waste Manag. Res.* **2018**, *36*, 197–199, <https://doi.org/10.1177/0734242X18758820>.
3. Alshehri, A.A.; Malik, M.A. Biogenic fabrication of ZnO nanoparticles using *Trigonella foenum-graecum* (Fenugreek) for proficient photocatalytic degradation of methylene blue under UV irradiation. *J. Mater. Sci.: Mater. Electron.* **2019**, *30*, 16156–16173, <https://doi.org/10.1007/s10854-019-01985-8>.
4. Han, C.; Andersen, J.; Pillai, S.C.; Fagan, R.; Falaras, P.; Byrne, J.A.; Dunlop, P.S.M.; Choi, H.; Jiang, W.; O’Shea, K.; Dionysiou, D.D. Chapter Green Nanotechnology: Development of Nanomaterials for Environmental and Energy Applications. In *Sustainable Nanotechnology and the Environment: Advances and Achievements*; ACS Symposium Series; American Chemical Society: **2013**; Volume 1124, pp. 201–229, <https://doi.org/10.1021/bk-2013-1124.ch012>.

5. Singh, P.; Kaur, N.; Khunger, A.; Kaur, G.; Kumar, S.; Kaushik, A.; Chaudhary, G.R. Green-monodispersed Pd-nanoparticles for improved mitigation of pathogens and environmental pollutant. *Mater. Today Commun.* **2022**, *30*, 103106, <https://doi.org/10.1016/j.mtcomm.2021.103106>.
6. Khin, M.M.; Nair, A.S.; Babu, V.J.; Murugan, R.; Ramakrishna, S. A review on nanomaterials for environmental remediation. *Energy Environ. Sci.* **2012**, *5*, 8075-8109, <https://doi.org/10.1039/c2ee21818f>.
7. Rónavári, A.; Igaz, N.; Adamecz, D.I.; Szerencsés, B.; Molnar, C.; Kónya, Z.; Pfeiffer, I.; Kiricsi, M. Green Silver and Gold Nanoparticles: Biological Synthesis Approaches and Potentials for Biomedical Applications. *Molecules* **2021**, *26*, 844, <https://doi.org/10.3390/molecules26040844>.
8. Jabbarzadeh, Z.; Khosh-Khui, M. Factors affecting tissue culture of Damask rose (*Rosa damascena* Mill.). *Sci. Hortic.* **2005**, *105*, 475-482, <https://doi.org/10.1016/j.scienta.2005.02.014>.
9. Dhar, G.; Akther, S.; Sultana, A.; May, U.; Islam, M.M.; Dhali, M.; Sikdar, D. Effect of extraction solvents on phenolic contents and antioxidant capacities of *Artocarpus chaplasha* and *Carissa carandas* fruits from Bangladesh. *J. Appl. Biol. Biotechnol.* **2017**, *5*, 39-44, <https://doi.org/10.7324/JABB.2017.50307>.
10. Dintcheva, N.T.; Morici, E. Recovery of Rose Flower Waste to Formulate Eco-Friendly Biopolymer Packaging Films. *Molecules* **2023**, *28*, 3165, <https://doi.org/10.3390/molecules28073165>.
11. Nasir, M.H.; Nadeem, R.; Akhtar, K.; Hanif, M.A.; Khalid, A.M. Efficacy of modified distillation sludge of rose (*Rosa centifolia*) petals for lead(II) and zinc(II) removal from aqueous solutions. *J. Hazard. Mater.* **2007**, *147*, 1006-1014, <https://doi.org/10.1016/j.jhazmat.2007.01.131>.
12. Tsanaktisidis, C.G.; Tamoutsidis, E.; Kasapidis, G.; Itziou, A.; Ntina, E. Preliminary Results on Attributes of Distillation Products of the Rose *Rosa damascene* as a Dynamic and Friendly to the Environment Rural Crop. *APCBEE Procedia* **2012**, *1*, 66-73, <https://doi.org/10.1016/j.apcbee.2012.03.012>.
13. Younis, I.Y.; El-Hawary, S.S.; Eldahshan, O.A.; Abdel-Aziz, M.M.; Ali, Z.Y. Green synthesis of magnesium nanoparticles mediated from *Rosa floribunda* charisma extract and its antioxidant, antiaging and antibiofilm activities. *Sci. Rep.* **2021**, *11*, 16868, <https://doi.org/10.1038/s41598-021-96377-6>.
14. de Nijs, E.A.; Maas, L.M.E.; Bol, R.; Tietema, A. Assessing the potential of co-composting rose waste as a sustainable waste management strategy: Nutrient availability and disease control. *J. Clean. Prod.* **2023**, *399*, 136685, <https://doi.org/10.1016/j.jclepro.2023.136685>.
15. Slavov, A.; Denev, P.; Panchev, I.; Shikov, V.; Nenov, N.; Yantcheva, N.; Vasileva, I. Combined recovery of polysaccharides and polyphenols from *Rosa damascena* wastes. *Ind. Crops Prod.* **2017**, *100*, 85-94, <https://doi.org/10.1016/j.indcrop.2017.02.017>.
16. Rabbani, D.; Mahmoudkashi, N.; Mehdizad, F.; Shaterian, M. Green Approach to Wastewater Treatment by Application of *Rosa damascena* Waste as Nano-Biosorbent. *Int. J. Environ. Sci. Technol.* **2016**, *9*, 121-130, <https://doi.org/10.3923/jest.2016.121.130>.
17. Aldeen, T.S.; Mohamed, H.E.A.; Maaza, M. ZnO nanoparticles prepared via a green synthesis approach: Physical properties, photocatalytic and antibacterial activity. *J. Phys. Chem. Solids* **2022**, *160*, 110313, <https://doi.org/10.1016/j.jpcs.2021.110313>.
18. Ngom, I.; Ngom, B.D.; Sackey, J.; Khamlich, S. Biosynthesis of zinc oxide nanoparticles using extracts of *Moringa Oleifera*: Structural & optical properties. *Mater. Today: Proc.* **2021**, *36*, 526-533, <https://doi.org/10.1016/j.matpr.2020.05.323>.
19. Raha, S.; Ahmaruzzaman, d. ZnO nanostructured materials and their potential applications: progress, challenges and perspectives. *Nanoscale Adv.* **2022**, *4*, 1868-1925, <https://doi.org/10.1039/D1NA00880C>.
20. Ahmadi, R.; Es-haghi, A.; Zare-Zardini, H.; Taghavizadeh Yazdi, M.E. Nickel oxide nanoparticles synthesized by Rose hip extract exert cytotoxicity against the HT-29 colon cancer cell line through the caspase-3/caspase-9/Bax pathway. *Emerg. Mater.* **2023**, *6*, 1877-1888, <https://doi.org/10.1007/s42247-023-00572-2>.
21. Wojnarowicz, J.; Chudoba, T.; Lojkowski, W. A Review of Microwave Synthesis of Zinc Oxide Nanomaterials: Reactants, Process Parameters and Morphologies. *Nanomaterials* **2020**, *10*, 108, <https://doi.org/10.3390/nano10061086>.
22. Adraoui, I.; Mamouni, R.; Saffaj, N.; Achemchem, F. Eco-friendly synthesis of zinc oxide nanoparticles using saffron extract and their photocatalytic and antibacterial activities. *J. Mater. Res.* **2023**, *38*, 2874-2884, <https://doi.org/10.1557/s43578-023-01024-7>.
23. Anvekar, T.S.; Chari, V.R.; Kadam, H. Green Synthesis of ZnO Nanoparticles, its Characterization and Application. *Mat. Sci. Res. India* **2017**, *14*, 153-157, <https://doi.org/10.13005/msri/140211>.

24. Rambabu, K.; Bharath, G.; Banat, F.; Show, P.L. Green synthesis of zinc oxide nanoparticles using *Phoenix dactylifera* waste as bioreductant for effective dye degradation and antibacterial performance in wastewater treatment. *J. Hazard. Mater.* **2021**, *402*, 123560, <https://doi.org/10.1016/j.jhazmat.2020.123560>.
25. Barzinjy, A.A.; Azeez, H.H. Green synthesis and characterization of zinc oxide nanoparticles using *Eucalyptus globulus* Labill. leaf extract and zinc nitrate hexahydrate salt. *SN Appl. Sci.* **2020**, *2*, 991, <https://doi.org/10.1007/s42452-020-2813-1>.
26. Gurusamy, M.; Sellavel, M.; Kuppuvelsamy, V. A sustainable green synthesis for photocatalytic and antibacterial activity of zinc oxide nanoparticles using *Cucumis maderaspatanus* leaf extract. *Desalin. Water Treat.* **2024**, *319*, 100457, <https://doi.org/10.1016/j.dwt.2024.100457>.
27. Irede, E.L.; Awoyemi, R.F.; Owolabi, B.; Aworinde, O.R.; Kajola, R.O.; Hazeez, A.; Raji, A.A.; Ganiyu, L.O.; Onukwuli, C.O.; Onivefu, A.P.; Ifijen, I.H. Cutting-edge developments in zinc oxide nanoparticles: synthesis and applications for enhanced antimicrobial and UV protection in healthcare solutions. *RSC Adv.* **2024**, *14*, 20992-21034, <https://doi.org/10.1039/D4RA02452D>.
28. Ait Baih, M.; Saffaj, H.; Aziz, K.; Bakka, A.; El baraka, N.; Zidouh, H.; Mamouni, R.; Saffaj, N. Statistical optimization of the elaboration of ceramic membrane support using Plackett-Burman and response surface methodology. *Mater. Today: Proc.* **2022**, *52*, 128-136, <https://doi.org/10.1016/j.matpr.2021.11.269>.
29. Maghsoudy, N.; Azar, P.A.; Tehrani, M.S.; Husain, S.W.; Larijani, K. Biosynthesis of Ag and Fe nanoparticles using *Erodium cicutarium*; study, optimization, and modeling of the antibacterial properties using response surface methodology. *J. Nanostruct. Chem.* **2019**, *9*, 203-216, <https://doi.org/10.1007/s40097-019-0311-z>.
30. Seetawan, U.; Jugsujinda, S.; Seetawan, T.; Ratchasin, A.; Euvananont, C.; Junin, C.; Thanachayanont, C.; Chainaronk, P. Effect of calcinations temperature on crystallography and nanoparticles in ZnO disk. *Mater. Sci. Appl.* **2011**, *2*, 1302-1306, <https://doi.org/10.4236/msa.2011.29176>.
31. Bhapkar, A.R.; Bham, S. A review on ZnO and its modifications for photocatalytic degradation of prominent textile effluents: Synthesis, mechanisms, and future directions. *J. Environ. Chem. Eng.* **2024**, *12*, 112553, <https://doi.org/10.1016/j.jece.2024.112553>.
32. Thirumalaisamy, R.; Subramanian, A.; Shanmugam, M. Optimization of zinc oxide nanoparticles biosynthesis from *Crateva adansonii* using Box-Behnken design and its antimicrobial activity. *Chem. Data Collect.* **2020**, *30*, 100581, <https://doi.org/10.1016/j.cdc.2020.100581>.
33. Es-haghi, A.; Taghavizadeh Yazdi, M.E.; Sharifalhosseini, M.; Baghani, M.; Yousefi, E.; Rahdar, A.; Baino, F. Application of Response Surface Methodology for Optimizing the Therapeutic Activity of ZnO Nanoparticles Biosynthesized from *Aspergillus niger*. *Biomimetics* **2021**, *6*, 34, <https://doi.org/10.3390/biomimetics6020034>.
34. Suryanarayana, C.; Norton, M.G. Crystal Structure Determination. II: Hexagonal Structures. In X-Ray Diffraction: A Practical Approach, Suryanarayana, C., Norton, M.G., Eds.; Springer US: Boston, MA, **1998**; pp. 125-152, https://doi.org/10.1007/978-1-4899-0148-4_5.
35. Agarwal, H.; Venkat Kumar, S.; Rajeshkumar, S. A review on green synthesis of zinc oxide nanoparticles – An eco-friendly approach. *Resource-Efficient Technol.* **2017**, *3*, 406-413, <https://doi.org/10.1016/j.reffit.2017.03.002>.
36. Scherrer, P. Bestimmung der inneren Struktur und der Größe von Kolloidteilchen mittels Röntgenstrahlen. In Kolloidchemie Ein Lehrbuch, Zsigmondy, R., Ed.; Springer Berlin Heidelberg: Berlin, Heidelberg, **1912**; pp. 387-409, https://doi.org/10.1007/978-3-662-33915-2_7.
37. Shashanka, R. Investigation of optical and thermal properties of CuO and ZnO nanoparticles prepared by Crocus Sativus (Saffron) flower extract. *J. Iran. Chem. Soc.* **2021**, *18*, 415-427, <https://doi.org/10.1007/s13738-020-02037-3>.
38. Aparna, Y.; Rao, K.V.; Subbarao, P.S. Preparation and Characterization of CuO Nanoparticles by Novel Sol-Gel Technique. *J. Nano- Electron. Phys.* **2012**, *4*, 03005.
39. Izgis, H.; Ilhan, E.; Kalkandelen, C.; Celen, E.; Guncu, M.M.; Turkoglu Sasmazel, H.; Gunduz, O.; Ficai, D.; Ficai, A.; Constantinescu, G. Manufacturing of Zinc Oxide Nanoparticle (ZnO NP)-Loaded Polyvinyl Alcohol (PVA) Nanostructured Mats Using *Ginger Extract* for Tissue Engineering Applications. *Nanomaterials* **2022**, *12*, 3040, <https://doi.org/10.3390/nano12173040>.
40. Kołodziejczak-Radzimska, A.; Jesionowski, T. Zinc Oxide—From Synthesis to Application: A Review. *Materials* **2014**, *7*, 2833-2881, <https://doi.org/10.3390/ma7042833>.

41. Rajendrachari, S.; Ceylan, K.B. The activation energy and antibacterial investigation of spherical Fe₃O₄ nanoparticles prepared by *Crocus sativus* (Saffron) flowers. *Biointerface Res. Appl. Chem.* **2020**, *10*, 5951–5959, <https://doi.org/10.33263/briac104.951959>.
42. Azizi, A.; Kazemi, M. Green synthesis of zinc oxide magnetic nanocomposite via zinc electroplating effluent: Its characterization and application as a photocatalyst. *Results Opt.* **2024**, *16*, 100698, <https://doi.org/10.1016/j.rio.2024.100698>.
43. Du, J.; Al-Huqail, A.; Cao, Y.; Yao, H.; Sun, Y.; Garaleh, M.; El Sayed Massoud, E.; Ali, E.; Assilzadeh, H.; Escorcia-Gutierrez, J. Green synthesis of zinc oxide nanoparticles from *Sida acuta* leaf extract for antibacterial and antioxidant applications, and catalytic degradation of dye through the use of convolutional neural network. *Environ. Res.* **2024**, *258*, 119204, <https://doi.org/10.1016/j.envres.2024.119204>.
44. Munshi, G.H.; Ibrahim, A.M.; Al-Harbi, L.M. Inspired Preparation of Zinc Oxide Nanocatalyst and the Photocatalytic Activity in the Treatment of Methyl Orange Dye and Paraquat Herbicide. *Int. J. Photoenergy* **2018**, *2018*, 5094741, <https://doi.org/10.1155/2018/5094741>.

Publisher's Note & Disclaimer

The statements, opinions, and data presented in this publication are solely those of the individual author(s) and contributor(s) and do not necessarily reflect the views of the publisher and/or the editor(s). The publisher and/or the editor(s) disclaim any responsibility for the accuracy, completeness, or reliability of the content. Neither the publisher nor the editor(s) assume any legal liability for any errors, omissions, or consequences arising from the use of the information presented in this publication. Furthermore, the publisher and/or the editor(s) disclaim any liability for any injury, damage, or loss to persons or property that may result from the use of any ideas, methods, instructions, or products mentioned in the content. Readers are encouraged to independently verify any information before relying on it, and the publisher assumes no responsibility for any consequences arising from the use of materials contained in this publication.